

# Determination of Optimal Row Spacing for a Staggered Cross-Pin Array in a Turbine Blade Cooling Passage

E. E. DONAHOO<sup>a,\*</sup>, C. CAMCI<sup>b</sup>, A. K. KULKARNI<sup>c</sup> and A. D. BELEGUNDU<sup>d</sup>

<sup>a</sup>Student Member ASME,

<sup>b</sup>Associate Professor of Aerospace Engineering,

<sup>c</sup>Professor of Mechanical Engineering, Member ASME,

<sup>d</sup>Professor of Mechanical Engineering, Member ASME, The Pennsylvania State University,  
University Park, PA 16802, USA

(Received 26 April 1999; In final form 4 June 1999)

Crosspin configurations are of interest in turbine blade design due to the enhanced cooling they provide. In addition, crosspins which extend from the walls of hollow blades provide structural integrity and stiffness to the blade itself. Numerous crosspin shapes and arrangements are possible, but only certain combinations offer high heat transfer capability while maintaining low overall total pressure loss. This study presents results from 2-D numerical simulations of coolant airflow through a turbine blade internal cooling passage. The simulations model viscous flow and heat transfer over circular pins in a staggered arrangement of varying pin spacing. Preliminary analysis over a wide range of Reynolds numbers indicates existence of an optimal spacing for which maximum heat transfer and minimum total pressure drop occurs. Pareto plots, which graphically identify the optimum data points with multiple optimization parameters, were obtained for a range of Reynolds numbers and streamwise spacings in a staggered crosspin arrangement. There is a steady increase in crosspin heat transfer up to a certain number of rows, then a gradual decrease in heat transfer in subsequent rows. Knowledge obtained from such findings can be used to determine the number of crosspins used, as well as the ultimate pin arrangement.

**Keywords:** Optimization; Turbine Blades; Cooling Passage; Crosspins; Pin fins

## INTRODUCTION

Strenuous demands are put on gas turbine blades operating in modern engines. Improvements in engine performance are closely related to increases

in the tolerance level of turbine inlet temperatures. The ability to operate at increasingly high temperatures has been a result of both improvements in materials capability to endure high thermal loads and advances in cooling schemes for hot

\* Corresponding author.

section components. Air-cooled turbine blades have made high cycle temperatures possible, resulting in high specific power. In the immediate future, it is most likely that air-cooled turbine blades will continue to be the solution for handling the higher turbine inlet temperatures with optimization of the design being necessary.

Recently, crosspins have been used in turbine blade coolant flow channels in order to enhance its cooling characteristics as illustrated in Figure 1. The crosspin itself is a cylindrical rod extending from the passage walls, and such pins are predominantly located near the blade's trailing edge. These pins affect the coolant flow negotiating around them in three ways: (i) they increase the total heat transfer surface area within the passage, thus leading to increased convection heat transfer; (ii) their staggered arrangement forces coolant air to travel a more tumultuous path, increasing the

turbulence level of the flow, resulting in greater convection cooling, and (iii) the presence of pins also presents added blockage to the flow, introducing a total pressure loss to the flow, which is undesirable for a given pressure head available from the compressor. Hence, the design of a pin arrangement requires optimization of certain parameters to ensure both desirable heat transfer and acceptable total pressure losses.

Previous studies have shown that longitudinal pin spacing indeed affects the overall heat transfer characteristics and total pressure drop. Peng (1983) conducted studies on crosspins, which extend the full height of the channel, and pin fins that extend only partially into the channel. He found experimental values for the heat transfer coefficient using the Colbourn factor and concluded that pin spacing affects partial pin fins slightly more than crosspins. Armstrong and Winstanley (1988) reviewed studies on local and array-averaged heat transfer in converging flow channels with a staggered pin alignment, and found that pin fin heat transfer averaged over the array appears to vary with Reynolds number to a power between 0.6 and 0.7, depending on pin height-to-diameter ratio,  $H/D$ . Effectiveness of pin fin arrays has also been studied by Metzger *et al.* (1982, 1984); Van Fossen (1981, 1984) and Chyu (1990, 1996). The objective of the present study is to derive an optimum pin spacing based on the detailed computation of heat flux and total pressure drop that can later be used in the design of pin arrangements and shape.

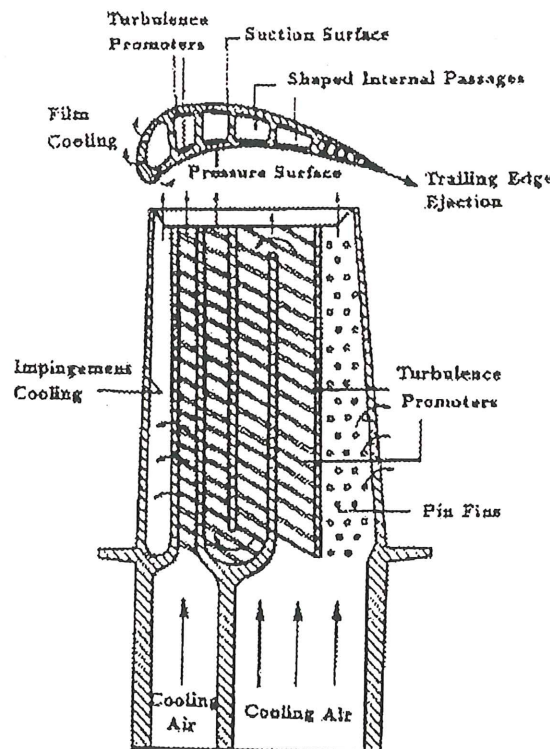


FIGURE 1 Turbine blade internal cooling passage (Zhang *et al.*, 1993).

## COOLANT PASSAGE MODEL

### Physical Model

Sophisticated cooling schemes employing complex passage-way designs (Fig. 1) have been used to maintain turbine blades operating under extreme conditions to stay within tolerable thermal limits. In this study, the domain itself consists of 10 rows of staggered circular crosspins (Fig. 2) within the

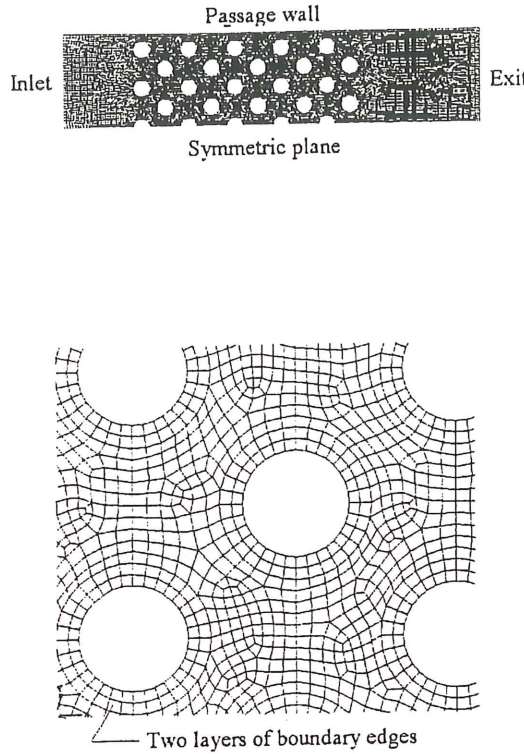


FIGURE 2 Top figure is a finite element mesh of the coolant passage. Bottom figure is a magnified view of the near wall grid that consists of two layers of structured elements, or boundary edges. The boundary edges are used near the crosspin surfaces and passage wall, then transitions into an unstructured grid.

turbine blade cooling passage. Figure 2 shows the finite element mesh using an unstructured grid of the cooling passage. However, close to the crosspin surface, two layers of a structured grid was used to accurately capture the sharp flow gradients in the near-wall region using special wall elements. Further out away from the pin walls, the grid transitioned into an unstructured grid to better handle the voids and irregular shape openings presented. A grid independence study was performed to determine what mesh density yielded less than 1% change in the flow solutions for velocity, pressure, and heat flux. Due to symmetry, only one-half the passage is modelled. The top and bottom planes represent the channel wall and a symmetry plane respectively.

### Mathematical Model

The current study uses a general purpose viscous flow solver to simulate the flow and heat transfer inside the turbine blade passage (FIDAP, 1993). Using a Galerkin finite element procedure to the stationary Navier-Stokes equations, a set of non-linear algebraic equations is obtained and represented in matrix form as:

$$K(u) = F \quad (1)$$

where  $K$  is the global matrix system,  $u$  is the global vector of unknowns (velocities, pressures, and temperatures) and  $F$  is a vector which includes the effects of body forces and boundary conditions. The numerical simulations of the flowfield inside a turbine blade passage involves solving the momentum and energy equations. In this problem, the momentum equation does not strongly depend on the temperature field, and is thus considered a weakly coupled problem. In such flows, the momentum equation can be solved independently of the other scalar equations, followed by the solution of the energy equation with a known velocity field.

A standard two-equation  $k - \varepsilon$  turbulence model is employed to represent the turbulent eddies and vortex mixing associated with flow through a pin fin array. In the  $k - \varepsilon$  turbulence model, the turbulence field is characterized in terms of two variables: the turbulent kinetic energy,  $k$ , defined as

$$k = \frac{1}{2} \overline{u_i u_i} \quad (2)$$

and the viscous dissipation rate of turbulent kinetic energy,  $\varepsilon$ .

$$\varepsilon = \nu \overline{u_{i,j} u_{i,j}}. \quad (3)$$

The unknown variables become  $(u_i, p, T, k, \varepsilon)$  and the corresponding field equations are: continuity,

$$u_{i,j} = 0 \quad (4)$$

momentum,

$$\rho_o \left( \frac{\partial u_i}{\partial t} + u_j u_{i,j} \right) = -p_{,i} + \rho_o f_i + [\bar{u}(u_{i,j} + u_{j,i})_j] \quad (5)$$

energy,

$$\rho_o c_p \left( \frac{\partial T}{\partial t} + u_j T_{,j} \right) = (\lambda T_{,j})_j + \mu \Phi + H \quad (6)$$

transport of turbulent kinetic energy,

$$\begin{aligned} \rho_o \left( \frac{\partial k}{\partial t} + u_j k_{,j} \right) &= \left( \mu_o + \frac{\mu_t}{\sigma_k} k_{,j} \right)_j + \mu_t \Phi \\ &+ \mu_t g_i \left( \frac{\beta_T}{\sigma_t} T_{,j} \right) - \rho_o \varepsilon \end{aligned} \quad (7)$$

transport of viscous dissipation rate,

$$\begin{aligned} \rho_o \left( \frac{\partial \varepsilon}{\partial t} + u_j \varepsilon_{,j} \right) &= \left( \mu_o + \frac{\mu_t}{\sigma_\varepsilon} \varepsilon_{,j} \right) + c_1 \frac{\varepsilon}{k} \mu_t \Phi \\ &+ c_1 (1 - c_3) \frac{\varepsilon}{k} g_j \left( \frac{\mu_t}{\sigma_t} \beta_r T_{,j} \right) \\ &- \rho_o c_2 \frac{\varepsilon^2}{k}. \end{aligned} \quad (8)$$

where the eddy viscosity take the form,

$$\mu_t + \rho_o c_\mu \frac{k^2}{\varepsilon}. \quad (9)$$

The computational domain modelling of the turbine coolant passage consists of an inlet, outlet, wall, and symmetry plane. The flowfield in the streamwise direction is considered symmetric about the centerline, so only one-half the passage is modelled. At the inlet, uniform velocity ( $U^* = U/U_i = 1$ ) and uniform temperature ( $T^* = (T - T_b)/(T_s - T_b) = 0$  for coolant flow) profiles were given. Dirichlet boundary conditions for the turbulent kinetic energy,  $k$ , was employed. From the turbulence intensity defined as,

$$I = \frac{\sqrt{u'^2}}{u_\infty} \quad (10)$$

a value for inlet  $k$  can readily be obtained,

$$k = 1.5(Iu_\infty)^2 \quad (11)$$

where  $u_\infty$  is the characteristic freestream velocity. The turbulent dissipation rate at the inlet was then assigned numerical values using the expression,

$$\varepsilon = \rho c_\mu \frac{k^2}{R_\mu \mu} \quad (12)$$

where  $R_\mu = \mu_t/\mu$  is the ratio of the turbulent to laminar viscosities. For most typical flows,  $R_\mu \sim O(10) - O(100)$ . At the outlet and symmetry planes, Neumann (*i.e.*, zero gradient or zero flux) boundary conditions are most appropriate for  $k$  and  $\varepsilon$ .

Along the wall boundaries, the no slip boundary condition was imposed for velocity, while a constant profile ( $T^* = 1$  for hot walls) was imposed for temperature.

A one element thick layer of special elements is employed in the near wall region between the fully turbulent outer flowfield and the physical boundary. Specialized shape functions are used within these near wall elements that accurately capture sharp variations of mean flow variables. The transport equations of  $k$  and  $\varepsilon$  are not solved in the layer of near-wall elements; instead, van Driest mixing length approach is used to model the turbulent diffusivities of heat and momentum (FIDAP, 1993). While the computational domain for the mean flow equations extends to the solid boundary, the computational domain for the  $k$  and  $\varepsilon$  transport equations extends only to the top of the near-wall elements. Applying appropriate boundary conditions at the near-wall elements produces,

$$\frac{\partial k}{\partial n} = 0 \quad (13)$$

and

$$\varepsilon = \frac{(c_\mu^{1/2} k)^{1.5}}{k \delta} \quad (14)$$

which are representative of the equilibrium turbulence conditions in the near wall regions where  $k$  is a constant and the turbulence length scale,  $k^{1.5}/\varepsilon$ , varies linearly with normal distance from the wall. At the end of each iteration, this value of  $k$  is used to arrive at a characteristic turbulent velocity scale for the near wall region. This value determines the magnitudes of the local element Reynolds number, which in turn control the degree of skewing in the special basis functions, thus enabling an accurate resolution of the local near wall profiles.

### Numerical Procedure

Instead of using a fully coupled solution approach, which requires the formation of a global matrix including all the unknown degrees of freedom associated with the discretized problem, a segregated solution algorithm was used. For a segregated solver, direct formulation of a global matrix system is unnecessary. Instead, this matrix is decomposed into smaller sub-matrices each governing the nodal unknowns associated with only one conservation equation. These smaller sub-matrices are then solved in a sequential manner using direct Gaussian elimination.

### THE OPTIMIZATION PROBLEM

Finding a crosspin configuration design that yields both favorable heat transfer characteristics and total pressure drop can be considered an engineering problem of optimization. As with this particular study, different objectives may not be compatible; the variables that optimize one objective may be far from optimal for another. For example, variables affecting heat flux and total pressure drop include pin spacing, number of pins, pin size and shape, as well as passage curvature. Certain pin spacing may produce favorable cooling characteristics, which is one objective, but also produce unfavorable pressure drops, which is another objective.

The approach taken was to generate a set of feasible designs, and then select an optimal design based on heat flux and total pressure drop. The variable in this study is the longitudinal pin spacing,  $x$ , which is the distance between centers of two adjacent pins in the streamwise direction. Different pin spacings were modelled while holding all other design parameters constant (*i.e.*,  $Re_D$ , inlet flow temperature,  $T_i$ , pin diameter,  $D = 0.01$  m and transverse spacing,  $x_T$ ); thus the sole effect is to isolate one design variable, that being  $x$ . The transverse spacing,  $x_T$ , was held to a constant value of  $2.5 D$ . Fourteen values of  $(x/D)$  were investigated between 1.0 and 4.0. This was done for four values of Reynolds numbers: 1270, 3980, 7310 and 13800. The Reynolds numbers chosen were in conjunction with case studies used by Armstrong (1988). For flow regimes between  $10^3 < Re_D < 10^5$ , the boundary layers around the cylinders contain both laminar and turbulent regions; thus all case studies were modelled using a  $k - \varepsilon$  turbulence model.

## RESULTS AND DISCUSSION

### Flow Characteristics

A velocity vector plot for  $Re_D = 1270$  with  $x/D = 1.5$  is shown in Figure 3(a). All governing equations are nondimensionalized to provide a measure of the relative importance of various terms and identify dominant physical phenomena. Hence, the inlet velocity is scaled accordingly as  $U^* = U/U_i$ . For  $Re_D = 1270$ , this would correspond to an inlet velocity of  $U_i = 15.48$  m/s. The scale identifies the relative magnitudes of the velocity vectors. As Figure 3(a) illustrates coolant flow negotiating around the first row of fins, three distinct processes develop. First, as flow passes through the converging cross section presented by adjacent fins, a jet is formed, accelerating the flow to values approximately  $1.5 U^*$ . Second, behind the pins, formation of wakes generates small but discernable recirculating zones of relatively low

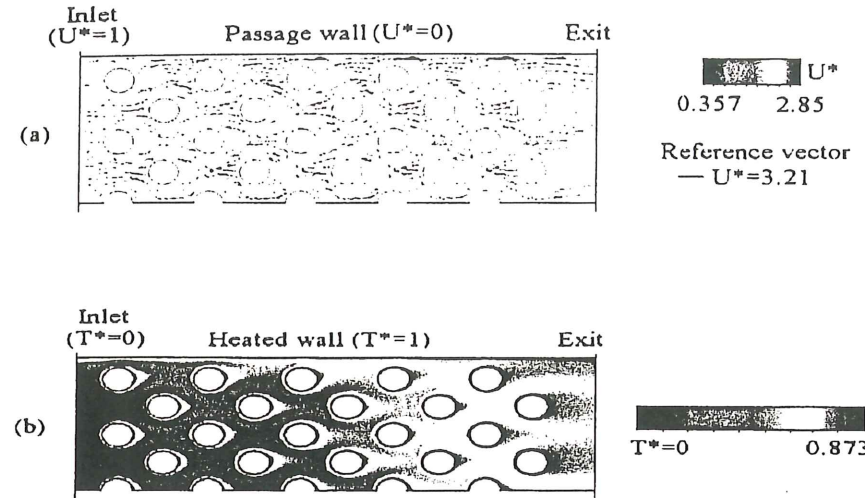


FIGURE 3 Plots for  $Re_D = 1270$  and  $x/D = 1.5$ . (a) Velocity vector plot where  $U^* = U/U_i$  ranges from  $U^* = 0.357$  (denoted by blue) to  $U^* = 3.21$  (denoted by red). (b) Temperature distribution where  $T^* = (T - T_i)/(T_s - T_i)$ .  $T^* = 0$  (blue contour levels) denotes inlet coolant air, while  $T^* = 1$  (red contour levels) denotes hot surfaces. (See Color Plate I).

velocity. Although the recirculation zones in the wakes have low velocities, high strain rates promote relatively high turbulence. The third process develops in subsequent rows, where the staggered pin arrangement forces the jet generated from the previous row to negotiate around another set of pins; in so doing, secondary jets are formed in converging cross sections. This staggered alignment creates a jet-wake interaction, where the outer region of the wake is entrained with accelerating flow negotiating the next set of pins. The accelerating flows coalesce from both sides, spawning new jets of equal magnitude as ones formed from the first row. The dynamics of these jet-wake interactions have a significant effect on the overall flowfield behavior. It is also apparent that the greatest acceleration occurs near the walls, where velocity magnitudes reach  $2.8U^*$ . The interference of wakes and growth of boundary layers cause the near wall velocity values to increase from approximately  $2.3U^*$  crossing row 1, to  $2.5U^*$  in row plane 2, and finally to values of  $2.8U^*$  in row plane 9.

Flows at  $Re_D = 3980$ , 7310 and 13800 respectively showed similar features (not presented here for brevity). At  $Re_D = 3980$ , the size of the wakes were uniform for pins within the core flow and

stretched approximately 0.4 diameter. For pins adjacent to the wall, the average wake size was larger, around 0.5 diameter. This difference in size is most likely due to local accelerations near the wall which is greater than anywhere else in the flow, producing a higher local Reynolds number. Thus, the effect of the near wall region on heat transfer can have significant implications in cross-pin design and arrangement.

Figure 3(b) is temperature contour plot of the same coolant flow as shown in Figure 3(a). The coolant flow enters with a nondimensional inlet temperature of  $T^* = 0$ , while the hot walls and fin surfaces are at a uniform temperature of  $T^* = 1$ . The flow enters from the left, and encounters the first row of pins, where large temperature gradients near the pin surfaces appear. It is here that the local heat flux is expected to be the highest. The wake is heated to about  $T^* = 0.37$ . The average core flow reaches a near uniform value by row 5, and increases steadily further from about  $T^* = 0.43$  to  $T^* = 0.77$ . Note the large temperature gradients along the wall continue to be significant until row 7. The exit flow is approximately at  $T^* = 0.75$ , indicating substantial heating of the coolant flow and substantial thermal energy

gained from convection cooling of fin surfaces. Knowledge of the local temperature distributions can also be helpful in determining whether thermal stresses generated within the passage are within tolerable limits.

Figure 4(a) is a turbulent kinetic energy contour plot with  $Re_D = 1270$  and  $x/D = 1.5$ . The flow enters with a freestream turbulence intensity of 1%. By rows 3 and 4, vortex shedding and subsequent vortex interaction from adjacent wakes become substantial enough to produce appreciable turbulent kinetic energy levels. The most intense turbulent kinetic energy seems to be produced in the forward part of the pins in rows 6–10 where vortex stretching is strong. In general, strong favorable pressure gradients are responsible for the production of significant vorticity at a solid surface, while adverse pressure gradients act as a sink of vorticity. Hence, the peak turbulent kinetic energy contour levels may be a result of rapid vorticity production along the forward pin section that "breaks away", becoming unstable and leading to significant activity by rows 4 and 5.

### Total Pressure Distributions

Figure 4(b) is a plot of the total pressure deviation with respect to  $p_{ref} = 100 \text{ kPa}$  for  $Re_D = 1270$  and

$x/D = 1.5$ . Table I lists the total pressure drop for each case studied, as well as the overall heat flux, the ratio of outlet to inlet temperatures, and min-max calculations (to be discussed later). For an adiabatic, frictionless flow, the total pressure would remain constant. However, for a viscous, turbulent flow, there will be losses due to viscous friction. Mean kinetic energy level of the flow is reduced by the viscous dissipation mechanism. This reduction is many times measurable as total pressure loss.

As the flow passes that last row of pins and exits the coolant passage, the total pressure levels off. Minimizing the total pressure loss is vital in crosspin design. Similar features were found for other  $x/D$  ratios for the range of Reynolds numbers studies.

### Pareto Curves

Pareto curves provide a graphical means of identifying optimum points having more than one objective function (the function to be maximized or minimized). Figure 5 is an illustration of a "generic" Pareto curve. The  $x$  and  $y$  axes correspond to the first and second objective functions ( $f_1$  and  $f_2$ ) to be optimized. If the goal is to maximize both parameters  $f_1$  and  $f_2$ , maximizing

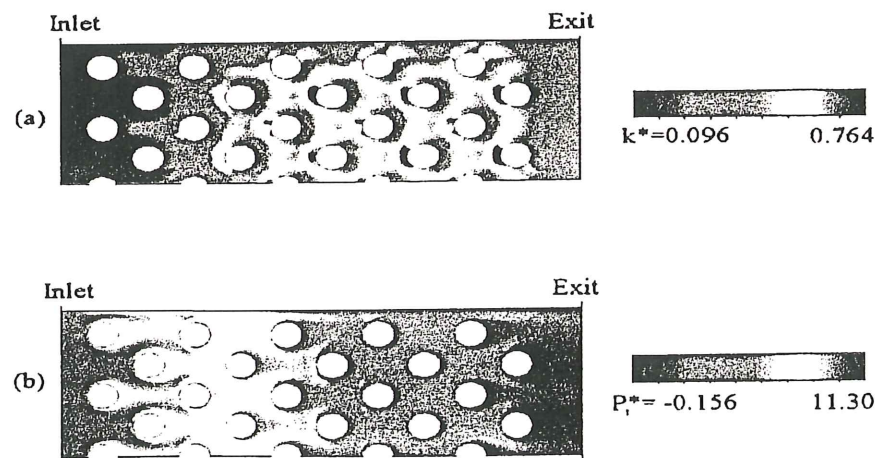


FIGURE 4 Plots for  $Re_D = 1270$  and  $x/D = 1.5$ . (a) Turbulent kinetic energy distribution where  $k^* = k/U_i^2$ . (b) Total pressure distribution with respect to  $p_{ref}$ , where  $p_i^* = p_i / 0.5\rho V^2$  and  $V$  = flow speed. (See Color Plate II).

TABLE I Passage flow test cases and results where  $\text{Max } \Delta f = \max(f_i(\tilde{x}) - f_i^*/f_i^{**})$ . (\*) denotes lowest values corresponding to optimum spacing

Set A					Set B			
$\text{Re}_D = 1270$					$\text{Re}_D = 3980$			
$M_i = 0.024$					$M_i = 0.076$			
$U_i = 15.48 \text{ m/s}$					$U_i = 48.51 \text{ m/s}$			
$T_i = 1000 \text{ K}$					$T_i = 1000 \text{ K}$			
$T_s = 1300 \text{ K}$					$T_s = 1300 \text{ K}$			
$x/D$	$q''(\text{W/cm}^2)$	$T_o/T_i$	$\Delta P_t (\text{kPa})$	Max $\Delta f$	$q''(\text{W/cm}^2)$	$T_o/T_i$	$\Delta P_t (\text{kPa})$	Max $\Delta f$
1.00	2.74	1.74	1.70	1.48	6.70	1.42	18.22	1.77
1.10	3.00	1.73	1.57	1.37	5.84	1.52	12.80	0.81
1.25	3.03	1.68	1.05	0.59	6.34	1.50	10.24	0.51
1.50	2.80	1.62	0.83	0.18	6.22	1.52	8.30	0.19
1.75	2.58	1.62	0.81	0.13	5.85	1.53	7.74	0.05
2.00	2.67	1.60	0.71	0.04*	5.34	1.53	7.90	0.19
2.25	2.55	1.60	0.71	0.08	5.62	1.56	6.84	0.01*
2.50	2.59	1.60	0.66	0.14	5.18	1.54	7.88	0.03
2.75	2.44	1.61	0.71	0.12	5.26	1.53	7.13	0.13
3.00	2.43	1.60	0.67	0.18	5.06	1.54	7.58	0.10
3.25	2.31	1.64	0.70	0.18	5.08	1.53	6.96	0.18
3.50	2.27	1.60	0.68	0.22	5.12	1.56	6.58	0.24
3.75	2.25	1.62	0.70	0.20	4.95	1.54	6.95	0.20
4.00	2.21	1.63	0.69	0.23	4.86	1.54	6.95	0.22
Set C					Set D			
$\text{Re}_D = 7310$					$\text{Re}_D = 13800$			
$M_i = 0.140$					$M_i = 0.265$			
$U_i = 89.10 \text{ m/s}$					$U_i = 168.20 \text{ m/s}$			
$T_i = 1000 \text{ K}$					$T_i = 1000 \text{ K}$			
$T_s = 1300 \text{ K}$					$T_s = 1300 \text{ K}$			
$x/D$	$q''(\text{W/cm}^2)$	$T_o/T_i$	$\Delta P_t (\text{kPa})$	Max $\Delta f$	$q''(\text{W/cm}^2)$	$T_o/T_i$	$\Delta P_t (\text{kPa})$	Max $\Delta f$
1.00	11.0	1.48	58.46	2.02	18.81	1.52	200.45	2.28
1.10	9.03	1.48	39.52	0.86	16.14	1.61	132.49	1.03
1.25	9.67	1.56	31.00	0.48	15.94	1.63	102.90	0.53
1.50	9.18	1.61	25.55	0.16	15.05	1.69	83.68	0.17
1.75	8.75	1.63	23.37	0.01*	14.21	1.70	76.30	0.01*
2.00	8.37	1.62	24.31	0.02	14.07	1.68	79.60	0.05
2.25	8.31	1.67	20.22	0.02	13.53	1.75	65.77	0.20
2.50	8.04	1.62	24.17	0.02	13.45	1.68	80.44	0.03
2.75	7.95	1.62	20.94	0.20	13.09	1.72	67.14	0.21
3.00	7.87	1.63	25.55	0.04	13.08	1.71	75.32	0.07
3.25	7.58	1.63	23.36	0.10	12.30	1.72	67.05	0.25
3.50	7.62	1.67	19.34	0.31	11.94	1.75	61.14	0.36
3.75	7.37	1.64	20.68	0.26	11.88	1.73	65.96	0.29
4.00	7.24	1.65	20.58	0.28	11.73	1.73	66.46	0.29

one may not necessarily maximize the other. The key is finding the compromise between both functions that would lead to an optimum point for both functions. For example, point A obtains the maximum value of  $f_1$ , but it also renders a minimal value for  $f_2$ . Point C obtains the

maximum value of  $f_2$ , but renders only the minimal value for  $f_1$ . The ideal point,  $(f_1^*, f_2^*)$ , maximizes both  $f_1$  and  $f_2$ . A *Pareto curve* is a curve drawn through a locus of points between A and C that correspond to "non-dominated" function values. For example, point B is "dominated" with

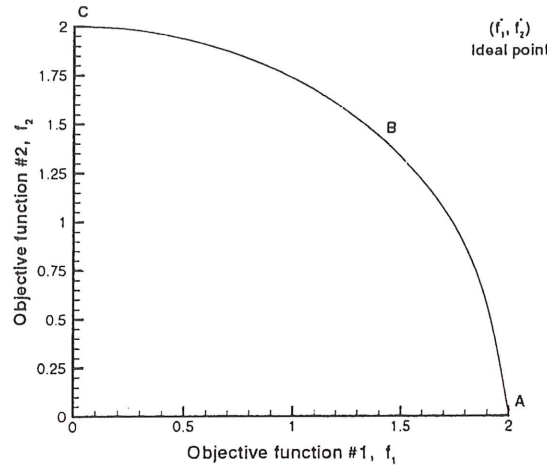
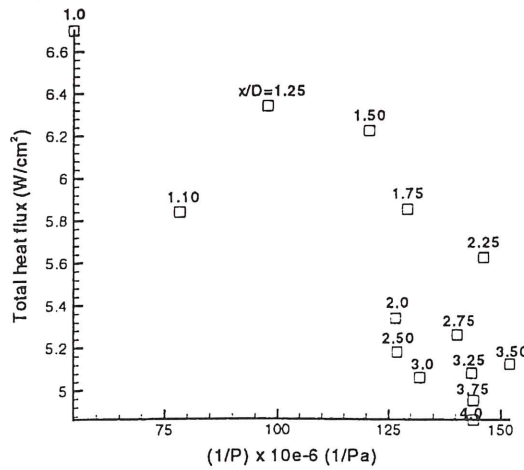


FIGURE 5 Generic Pareto curve.

respect to  $f_1$  and  $f_2$  by all point on the dotted curve. We may use the curve to determine a best compromise design by choosing the point closest to the ideal point.

Figure 6 is a Pareto plot of test cases run with  $Re_D = 3980$  at different crosspin spacings. Since minimizing the total pressure drop,  $\Delta p_r$ , is equivalent to maximizing  $1/\Delta p_r$ , both the passage heat flux,  $q''$ , and  $1/\Delta p_r$  are objectives that are to be maximized. For consistency, the total pressure drop was computed using the same upstream and downstream locations relative to the pin location:

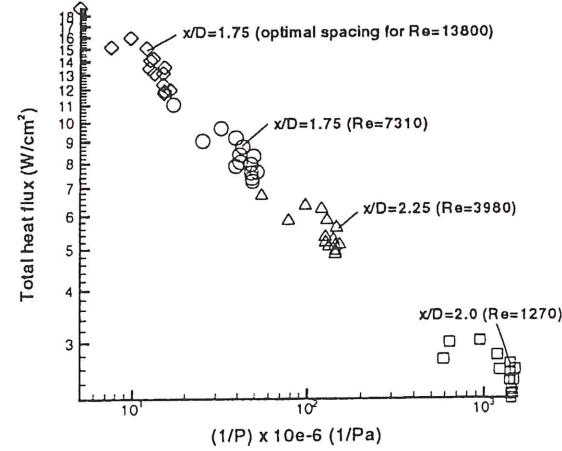
FIGURE 6 Pareto curve for  $Re_D = 3980$  and different cross-pin spacings.

five diameters upstream from the first row of fins, and eight diameters downstream from the last row. The total heat flux includes convection losses from all pin surfaces and the sidewall. The best candidate would be a point that maximizes  $q''$  while maintaining high values for  $1/\Delta p_r$ . Note that for  $x/D = 2.25$  to 4.0,  $1/\Delta p_r$  values do not differ significantly. Of these points,  $x/D = 2.25$  renders the highest heat flux, as shown in Table I. Hence, we can conclude that  $x/D = 2.25$  would be chosen as an optimum spacing for these flow conditions. To determine if  $x/D = 2.25$  agrees with a more rigorous definition of "best compromise", we considered the expression,

$$\text{minimize } \max \left( \frac{f_1(\tilde{x}) - f_1^*}{f_1^*}, \frac{f_2(\tilde{x}) - f_2^*}{f_2^*} \right). \quad (15)$$

where  $f_1^*$  represents the "best"  $f_1$  value, and  $f_2^*$  represents the "best"  $f_2$  value. Comparing the min-max values of each test case, the value of  $x/D = 2.25$  rendered the lowest value of 0.01 (see Tab. I). Thus, this would agree with the graphical solution depicted by Figure 6.

Figure 7 combines the Pareto distributions for  $Re_D = 1270$ , 3980, 7310 and 13800. An optimum spacing is not so clear from looking at the pareto distribution for  $Re_D = 1270$ , but it would seem

FIGURE 7 Pareto distributions for  $Re_D = 1270$ , 3980, 7310, 13800.

that  $x/D$  values between 2.0 and 4.0 are likely candidates. Computing the normalization for each case,  $x/D = 2.0$  rendered the best solution (see Tab. I). At  $Re_D = 7310$  and  $Re_D = 13800$ ,  $x/D = 1.75$  were optimal as shown in Figure 7. Thus, streamwise distances between 1.75 and 2.25 times the pin diameter can be starting grounds for designing pin arrangement that yield optimum cooling and pressure drop characteristics.

### Heat Flux Dependence on Row Location

Figure 8 shows the average heat flux from pins in each row with  $Re_D = 7310$ . There is an indication that maximum cooling occurs with certain rows, where it appears to be row 4 for  $x/D = 4$ , and row 5 for  $x/D = 2$ . This can be attributed to the fact that flow through the passage behaves similarly to flow within a heat exchanger with a turbulence grid. Turbulence levels build up as flow moves downstream, and then levels off. It is here that the convection cooling can be expected to reach a maximum. (It should be noted that experimental studies from Peng, 1983 of short 3-D crosspins with  $H/D = 1.0$  show maximum heat transfer occurs within the first three rows. The fact that maximum convection cooling occurs further

upstream for 3-D pins can be attributed to the presence of endwalls which enhances the development of a thermal boundary layer. Three dimensional endwall effects will be examined in a subsequent study.) Similar features were found at  $Re_D = 1270$ , 3980 and 13800. The number of possible designs and variables to examine is large, but this and future studies will provide useful information in determining optimum pin arrangements.

### Comparison with Past Experiments

This study presents results from a 2-D model, which assumes infinite length scales in the  $z$  direction. Of course, this has no physical significance since most turbine blades use  $H/D$  values of order 1. In order to interpret the results presented, it must be determined to what extent the 2-D results come close to documented experimental results or other 3-D models. Comparing results with Peng (1983), the Colbourn factor was calculated from the expression,

$$j = \frac{h}{G_{\max} c_p} \Pr^{2/3} \quad (16)$$

where  $h$  is the overall heat transfer coefficient within the passage channel,  $G_{\max}$  is the maximum mass flux per unit area, and  $c_p$  is the specific heat. The Colbourn factors computed were compared to experimental values from Peng's study, and shown in Figure 9. The Colbourn factor is proportional with a Stanton number obtained by using  $G_{\max}$  as the density-velocity product for a constant Prandtl number flow. Present 2-D computations (for large  $H/D$  values) are denoted by solid circles in Figure 9. The computed results agree very well with Peng's experiments for  $Re_D = 3980$ , 7310 and 13800. Experimental results show that aspect ratios of  $H/D$  from 19 down to 10 does not affect the overall heat transfer characteristics. In the specific  $H/D$  range ( $10 \leq H/D \leq 20$ ) three dimensional endwall flow physics does not interfere with

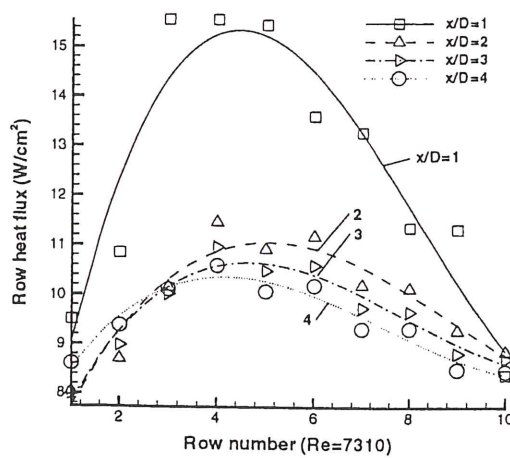


FIGURE 8 Pin averaged heat flux vs. row number for  $Re_D = 7310$ .

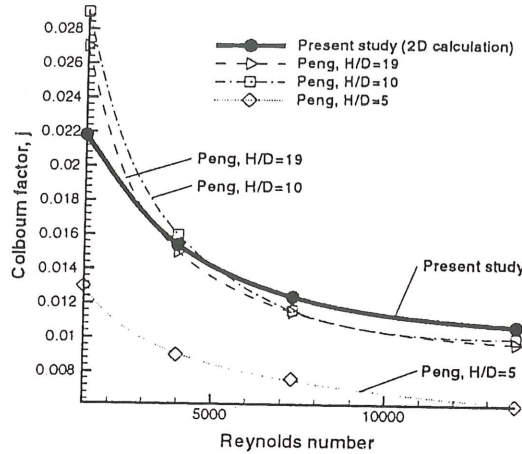


FIGURE 9 Comparison of Colbourn factors,  $j$ , with another study.

the midspan flow and heat transfer processes. Although this  $H/D$  range is not quite practical for present day gas turbine  $H/D$  values, the comparison shown in Figure 9 is important because it provides an excellent validation of the specific finite element procedure used in this study. A significant drop in the Colbourn factor obtained from Peng's experiments is also shown for a short aspect ratio of  $H/D = 5$ . Meaningful computation of Colbourn factors for short  $H/D$  ratios can be performed using a 3-D version of the numerical method presented in this paper. The current study establishes the foundation for the finite element method, an optimization technique, and experimental validation of the approach before a more time consuming larger scale, 3-D viscous flow heat transfer simulation including endwall effects is attempted.

The total pressure drop was also compared by evaluating the friction factor,  $f$ , expressed as

$$f = \frac{D_h \rho \Delta P}{8 L G^2 c_p} \quad (17)$$

Figure 10 shows the comparison of experimental friction factors from Peng's experiments and current computations. For  $Re_D = 3980, 7310$  and  $13800$  the computed average total pressure loss

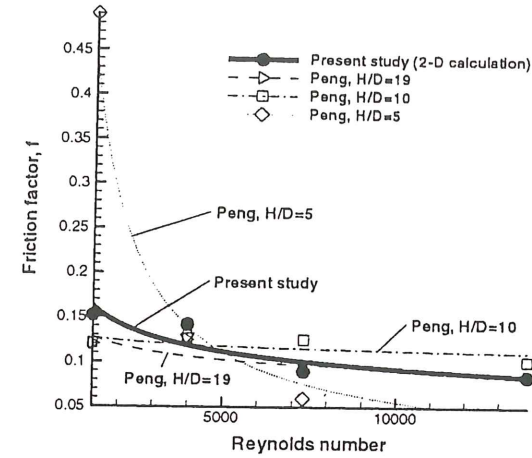


FIGURE 10 Comparison of friction factors,  $f$ , with another study.

agrees reasonably well Peng's experiments for  $H/D = 19$  and  $10$ . The results suggest that although an extremely accurate prediction of the viscous flow total pressure loss are not possible at this time, the current method provides a useful flow and heat transfer simulator tool for optimization purposes. Future optimization studies will focus on the 3-D contributions from the endwalls of the coolant passage in the range of  $0.5 \leq H/D \leq 3$ .

## CONCLUSIONS

This study presents results from 2-D numerical simulations of coolant flow through a turbine blade cooling passage. The primary focus was to develop an optimization strategy to find  $x/D$  values that yielded high convection cooling while rendering minimal total pressure losses. The effects of one design parameter, the longitudinal pin spacing,  $x$ , were investigated by varying  $x$  while holding all other parameters constant (*i.e.*,  $Re_D$ ,  $T_i$ ,  $D$  and  $x_T$ ). Fourteen values of  $(x/D)$  were investigated between 1.0 and 4.0 for four values of the Reynolds number: 1270, 3980, 7310 and 13800. It was found that for  $Re_D = 1270$  an optimum spacing of  $x/D = 2.0$  exists, while a

slightly higher value of  $x/D = 2.25$  is optimum for  $Re_D = 3980$ . For  $Re_D = 7310$  and  $Re_D = 13800$ ,  $x/D = 1.75$  is optimum. There are also certain row locations for which the heat flux reaches a maximum. The heat flux reaches a maximum between rows 4 and 6 for the range of  $x/D$  values and Reynolds numbers studied. There are two competing effects that are responsible for heat flux values reaching a maximum. Moving through the crosspin array, the driving force for heat transfer, which is the difference between the averaged pin surface temperature and the coolant fluid temperature, decreases, thus the averaged heat flux would be forced to decrease. However, the turbulent kinetic energy is increasing up to row 6, which enhances convection cooling. Initially, the effect of increasing the turbulent kinetic energy dominates over the effect of a diminished temperature difference, and the net effect is for the averaged heat flux to increase. However, by rows 4 and 5, increases in the turbulent kinetic energy become negligible, eventually leveling off, and the effect of a continually decreasing temperature difference becomes dominant, thus lowering the averaged heat flux values.

Since this was a 2-D numerical study, the criteria for which these findings are meaningful must be emphasized. From a comparison with Peng's experimental investigation of long and short crosspins, it can be comfortably stated that the author's findings agree well with the heat transfer and pressure drop characteristics for pins with  $H/D \geq 10$  for the range of Reynolds numbers studied. Shorter pins where  $H/D < 10$  may present three dimensional endwall effects that are not currently captured by the 2-D model. Furthermore, when subsequent 3-D simulations are undertaken, certain physical phenomena can be isolated that are not seen from the 2-D study. Thus the 2-D findings can serve as a baseline for which the flow physics can be compared to 3-D effects. A continuation of this optimization study considering 3-D endwall effects using short crosspins is under progress.

### Acknowledgements

The authors would like to thank the National Science Foundation Graduate Research Traineeship (NSF-GRT) Program in Environmentally Conscious Manufacturing at The Pennsylvania State University for partially funding this research and the Center for Academic Computing for the computing time made available.

### NOMENCLATURE

$A_{\min}$	minimum free flow area of test core
$D$	pin diameter
$D_h$	hydraulic diameter
$f$	friction coefficient
$h$	convection heat transfer coefficient, $h = q''/(T_s - T)$
$H$	pin height
$I$	turbulence intensity
$l_m$	mixing length
$L$	channel length
$k$	turbulent kinetic energy, ( $k^* = k/U_i^2$ )
$M_i$	inlet Mach number
$p_{\text{ref}}$	reference pressure = 100 kPa
$p_t$	total pressure, ( $p_t^* = p_t/0.5\rho V^2$ )
$\Pr$	Prandtl number
$q''$	heat flux within flow passage
$R_\mu$	ratio of turbulent to laminar viscosities
$Re_D$	Reynolds number = $\rho U_i D / \mu$
$T$	local static temperature
$T_s$	surface temperature
$T^*$	dimensionless temperature, $T^* = (T - T_i)/(T_s - T_i)$
$(T_o/T_i)$	ratio of outlet to inlet temperatures
$u'$	fluctuating velocity component
$u_\infty$	freestream velocity
$u_i$	mean velocity component
$U_i$	inlet flow velocity

$x^*$	streamwise distance between adjacent pin centers
$y^+$	dimensionless normal distance from wall

### Greek Letters

$\alpha$	relaxation factor
$\delta$	boundary layer thickness
$\Delta$	differential
$\varepsilon$	viscous dissipation rate
$\lambda$	thermal conductivity of air
$\eta$	pin efficiency
$\mu$	laminar viscosity
$\mu_t$	eddy viscosity
$\bar{\mu}$	total viscosity, $\bar{\mu} = \mu + \mu_t$
$\infty$	Freestream

### References

- Armstrong, J. and Winstanley, D. (1988) A Review of Staggered Array Pin Fin Heat Transfer for Turbine Cooling Applications. *ASME Journal of Heat Transfer*, **110**, 94–103.
- Brigham, B. A. and VanFossen, G. J. (1987) Length-to-Diameter Ratio and Row Number Effects in Short Pin Fin Heat Transfer. *ASME Journal of Engineering for Gas Turbines and Power*, **106**, 241–245.
- Chyu, M. K. (1990) Heat Transfer and Pressure Drop for Short Pin-Fin Arrays with Pin Endwall. *Journal of Heat Transfer*, **112**, 926–932.
- Chyu, M. K., Hsing, Y. C. and Natarajan, V. (1996) Convective Heat Transfer of Cubic Fin Arrays in a Narrow Channel. ASME Paper No. 96-GT-201.
- FIDAP 7.0 Tutorial Manual, 1993, Fluid Dynamics International, Inc., Chap. 7.
- Metzger, D. E. and Haley, S. W. (1982) Heat Transfer Experiments and Flow Visualization for Arrays of Short Pin Fins. ASME Paper No. 82-GT-138.
- Metzger, D. E. and Haley, S. W. (1984) Effects of Pin Shape and Array Orientation on Heat Transfer and Pressure Loss in Pin Fin Arrays. *Journal of Engineering for Gas Turbine and Power*, **106**, 252–257.
- Metzger, D. E. and Shepard, W. B. (1986) Row-Resolved Heat Transfer Variations in Pin Fin Arrays Including Effects of Non-Uniform Arrays and Flow Convergence. ASME Paper No. 86-GT-132.
- Panton, Ronald, L. (1984) Incompressible Flow. John Wiley & Sons, Inc., pp. 334–338.
- Peng, Y. (1983) Heat Transfer and Friction Characteristics of Pin Fin Cooling Configuration. *ASME Journal of Heat Transfer*, **83**, 1–6.
- Sparrow, E. M., Ramsey, J. M. and Altemani, C. A. C. (1992) Experiments on In-Line Pin Fin Arrays and Performance Comparisons with Staggered Arrays. *ASME Journal of Heat Transfer*, **102**, 44–50.
- VanFossen, G. J. (1981) Heat Transfer Coefficients for Staggered Arrays of Short Pin Fins. *ASME Journal of Engineering for Power*, **104**, 268–274.
- VanFossen, G. J. (1984) Heat Transfer Coefficients for Staggered Arrays of Short Pin Fins. *Journal of Engineering for Power*, **104**, 268–274.
- Zhang, Y. M., Han, J. C. and Parsons, J. A. (1993) Surface Heating Effect on Local Heat Transfer In a Rotating Two-Pass Square Channel With 60 Degree Angled Rib Turbulators. ASME Paper No. 93-GT-336, pp. 1–9.
- Zukauskas, A. A. (1992) Heat Transfer From Tubes in Cross Flow. *Adv. in Heat Transfer*, **8**, 116–133.